Multifaceted terahertz applications of parallel-plate waveguide: TE_1 mode

R. Mendis and D.M. Mittleman

Presented is a review of recent work by the authors in which the lowest-order transverse-electric (TE_1) mode of a parallel-plate waveguide (PPWG) is used for terahertz (THz) applications. This work adds a new dimension to the multitude of diverse THz applications made possible by PPWGs. Using the TE_1 mode, demonstration is presented of an ultra-low loss THz waveguide, a highly sensitive microfluidic sensor, a whispering-gallery mode waveguide, and an artificial dielectric with an effective refractive index less than unity.

Introduction: Exploitation of the parallel-plate-waveguide (PPWG) geometry has proved to be a major technological breakthrough for terahertz (THz) applications ever since the first demonstration of its use for low-loss, undistorted THz pulse propagation [1, 2]. Undistorted pulse propagation was achieved by exciting the waveguide's dominant transverse-electromagnetic (TEM) mode that exhibits virtually no group-velocity-dispersion (GVD) due to the absence of a low-frequency cutoff. This capability to propagate 'clean' THz pulses within a two-dimensional metallic environment has enabled numerous THz applications including pulse generation [3, 4], spectroscopy [5–7], sensing [8, 9], imaging [10, 11], signal processing [12], and even super-focusing [13].

Recently, we demonstrated THz pulse propagation by exciting the waveguide's lowest-order transverse-electric (TE_1) mode, which was not previously considered to be a viable wave-guiding option owing to the presence of a low-frequency cutoff. This cutoff causes spectral filtering and introduces high GVD that results in undesirable broadening and reshaping of the input THz pulses. Our recent work has shown, however, that it is possible to avoid these undesirable effects, so that the TE_1 mode is a viable option for efficient low-loss wave-guiding [14, 15]. We have also shown that one can achieve undistorted THz pulse propagation using the TE_1 mode with ultra-low ohmic losses in the dB/km range.

Moreover, use of the TE_1 mode opens up a whole new dimension to the capabilities offered by the PPWG. We have shown that it is possible to excite a simple resonant cavity integrated with a PPWG via the TE_1 mode. This cavity can be used as a microfluidic sensor with a refractive-index sensitivity of 3.7×10^5 nm/RIU (where RIU $\equiv$ refractive-index-units), the highest ever reported in any frequency range [16]. Originating from the TE_1 mode of a PPWG, we have shown excitation of whispering-gallery modes on concave metallic surfaces, thereby providing a new option for THz waveguides based on curved metallic surfaces [17]. Furthermore, we have shown how a PPWG operating in the TE_1 mode can be used as a two-dimensional (2D) artificial-dielectric medium, the refractive index of which can be tuned between zero and unity [18]. Using this artificial-dielectric concept we demonstrated several applications including a 'universal' THz spectral filter [19]. In the following Sections, we present some of our latest results.

Ultra-low loss waveguide: A typical TE_1-mode propagation behaviour in a PPWG is illustrated in Fig. 1. The input THz pulse is given in Fig. 1*a*, and the output through two 25.4 mm-long PPWGs with plate-separations of $b = 0.5$ mm and $b = 5$ mm are given in Figs. 1*b* and *c*, respectively. This demonstrates that although, in general, the output pulse is broadened and reshaped compared to the input pulse, as in Fig. 1*b*, it is in fact possible to avoid this dispersive behaviour by using a much larger value of b. It is well-known that the dispersion is caused by the presence of a low-frequency cutoff given by $f_c = c/(2b)$, where c is the velocity of light in free space. Therefore, by increasing b, we can lower the cutoff to an extent that it falls below the low-frequency end of the input spectrum, and thus diminish its effects on the propagation. For example, when $b = 5$ mm, $f_c = 30$ GHz, which is at the very low end of the bandwidth of the typical THz pulse used in our experiments.

In addition to reducing the GVD and helping to maintain the spectral integrity of propagating THz pulses, another advantage of increasing b is the consequent decrease in ohmic loss. This effect is illustrated in Fig. 2. For example, when b increases from 0.5 to 5 mm, by a factor of 10, the loss at 1 THz drops from 2.7×10^{-2} to 2.6×10^{-5} dB/cm (= 2.6 dB/km), a factor of more than 1000. This highly nonlinear behaviour can be attributed to the unique frequency dependence of the ohmic loss, which decreases with increasing frequency for all frequencies above cutoff. This frequency dependence is counter to the typical trend for ohmic (dissipative) losses in waveguides.

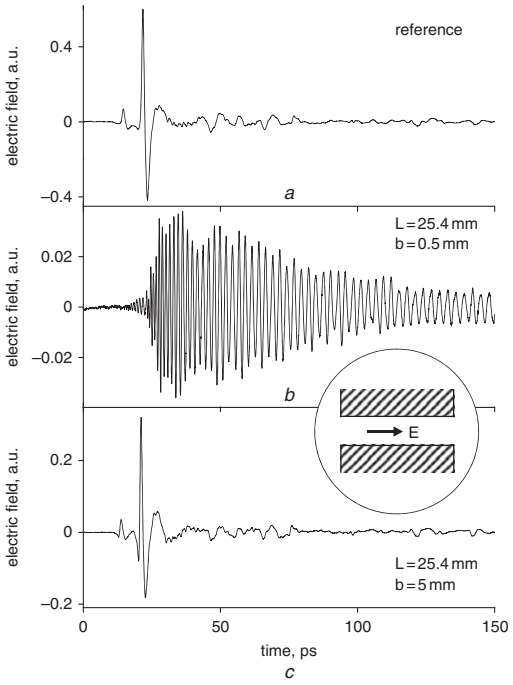

Fig. 1 *Time scans corresponding to (Fig. 1a) input reference, and TE_1-mode propagation in 25.4 mm long PPWG with (Fig. 1b) $b = 0.5$ mm, and (Fig. 1c) $b = 5$ mm*

Inset (circled): Excitation polarisation axis with respect to plate surfaces

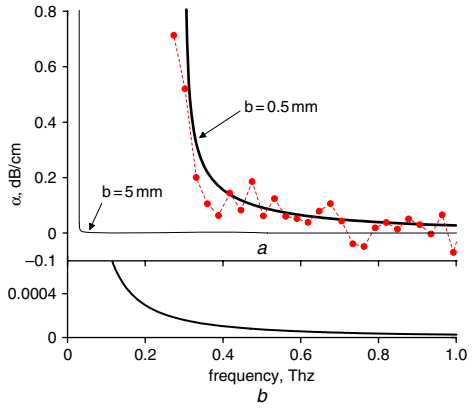

Fig. 2 *Attenuation constant for TE_1 mode, and baseline of theoretical curve*

a Attenuation constant for TE_1 mode

Theoretical thick and thin solid curves are for $b = 0.5$ mm and 5 mm, respectively. Red dots are experimental data

b Baseline of theoretical curve for $b = 5$ mm, on expanded vertical axis

One possible significant disadvantage in pushing the TE_1 cutoff to lower frequencies by increasing b is that the waveguide becomes overmoded. Since the cutoff frequencies of many higher-order modes now fall within the spectrum of the broadband input pulse, this could lead to multimode excitation. However, this problem can be overcome if the TE_1 mode is exclusively excited via mode-matching. By using an incident beam size equal to $0.7b$, it is possible to couple almost 99% of the incident power from a focused Gaussian beam into the TE_1 mode. For $b = 5$ mm, this corresponds to a reasonable THz beam size. As a result, we are able to easily demonstrate single TE_1 mode propagation (see Fig. 1*c*).

To make this a viable ultra-low loss wave-guiding technique suitable for long path lengths, one needs to tackle the issue of energy leakage due to diffraction in the unconfined (transverse) direction. The use of slightly concave metal plates can in principle eliminate this concern. The curved plates act as an effective lens waveguide, guaranteeing that the propagating mode never diffracts to the edges of the metal plates. Somewhat

surprisingly, this solution is predicted to be effective over a very wide spectral bandwidth [15].

Microfluidic sensor: In this work, we have shown that a rectangular groove machined into one plate of a PPWG can act as a resonant cavity that can be efficiently excited via the TE_1 mode. It is interesting to note that this simple cavity essentially does not couple to the TEM mode. Since the resonator can act as a channel for fluid flow, it can be easily integrated into a microfluidic platform for real-time refractive-index sensing.

The device geometry is illustrated in Fig. 3. The PPWG, consisting of two aluminium plates, is assembled with 1 mm-thick glass spacers. The groove machined into the lower plate slopes up at either end to contain the fluid under study (volume $\simeq$ 8 μl). The back-reflection of a HeNe laser beam is used to monitor the filling level. Fig. 4 shows the amplitude spectra corresponding to the propagated THz signals with and without a particular fluid filling the groove. For illustrative purposes, we use a linear alkane (undecane: $C_{11}H_{24}$), the THz spectroscopic properties of which are known [20]. Both spectra exhibit a cutoff at 0.15 THz, corresponding to the plate separation $b = 1$ mm. In the case of the empty groove, there is a strong narrow dip at 0.293 THz, caused by the empty resonant cavity. In the case of the filled groove, the resonance dip has shifted to a lower frequency owing to the higher refractive index inside the cavity. This dramatic red-shift is directly related to the refractive index of the material inside the resonator, and demonstrates how this system can be used as a refractive-index sensor.

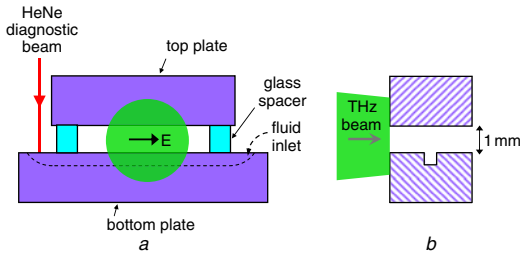

Fig. 3 *Input face of assembled PPWG, and axial cross-section of device*

a Input face of assembled PPWG (not to scale)
Dashed line on bottom plate shows longitudinal profile of groove machined into lower plate, forming resonant cavity. This groove, situated half-way between the input and output faces of the waveguide, has a nearly rectangular cross-section with width of 472 μm and depth of 412 μm. One uncovered end of the groove is used as the fluid inlet (right side), the other end is used for the optical diagnostic beam. Circular spot indicates input THz beam, which is smaller than width of plates. Glass spacers maintain 1 mm separation between plates
b Axial cross-section of device along direction of propagation showing transverse profile of groove on bottom plate
Propagation length of waveguide is 6.4 mm

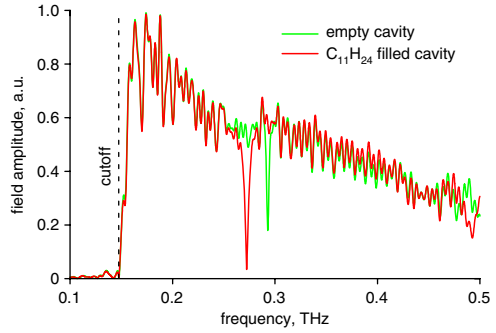

Fig. 4 *Amplitude spectra*

Amplitude spectra corresponding to output THz signals of waveguide with empty cavity (green curve) and filled cavity (red curve). For the latter, cavity is completely filled with liquid undecane ($C_{11}H_{24}$). The red shift in the resonance dip due to fluid filling is clearly evident in red curve. Both spectra show waveguide cutoff at 0.15 THz due to 1 mm plate separation

To investigate this possibility, we measured the resonance shifts for a series of linear-chain hydrocarbons with well-known (nearly frequency-independent) refractive indices in the THz range. Our measurements and subsequent numerical simulations indicated a quadratic dependence of the resonance shift as a function of the refractive index of the fluid. We derive the refractive-index sensitivity for liquids with an index of around 1.4 (our experimental range), in conventional units, to be $\Delta\lambda/\Delta n = 3.7 \times 10^5$ nm/RIU. This value is the highest ever reported in any frequency range for any optical refractive-index sensor [16].

Whispering-gallery modes: In analysing the concept of concave plates for wave guiding mentioned above, we relied on the understanding that the TE_1 mode can be described using a 'bouncing-plane-wave' picture. The TE_1 mode propagation is then analysed in terms of a travelling plane wave, continuously bouncing back and forth between the two metallic plates. A natural consequence of this is the possibility of guiding energy using only a single concave plate, provided there is enough curvature to sustain continuous reflections. This concept is analogous to the whispering gallery (WG) modes first demonstrated by Rayleigh, where sound waves were shown to cling to and follow a cylindrical surface [17].

Fig. 5 presents two overlapping THz output signals corresponding to the waveguide configurations (longitudinal cross-sections) shown in the two insets. The composite PPWG shown in the left inset has a 3 cm straight section followed by a semicircular section having radii of 7 and 8 cm for the inner and outer plates, respectively. The curved inner plate could be detached leaving the 25.1 cm-long curved outer plate and the straight PPWG section intact, as shown in the right inset. For both configurations, the TE_1 mode was initially excited in the 3 cm PPWG section. Remarkably, when the inner plate is detached, the main THz pulse of the output signal is almost indistinguishable from that of the composite. This indicates that the inner curved plate has minimal effect on the propagating THz signal, implying that energy is mostly concentrated near the outer plate in the curved section. We investigate this further, by forming a variable slit near the surface of the plate using a flat metal beam block at the input, centre (as shown in the inset), and output, along the curved path, and measuring the propagated signal. These results are shown in Fig. 6 and confirm that energy is confined within 10 mm from the plate surface, while being guided along the curved path.

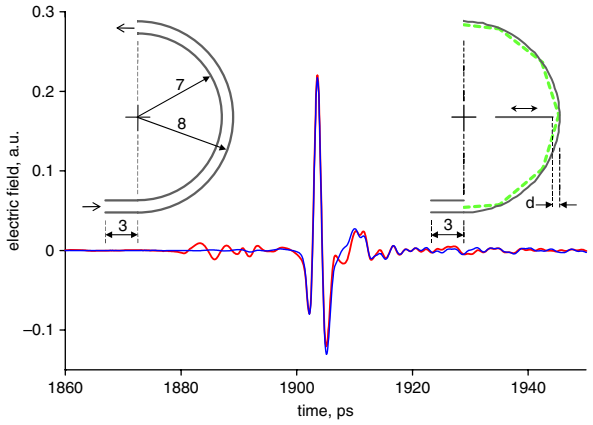

Fig. 5 *THz waveforms*

Blue trace is THz waveform corresponding to composite PPWG in left inset; red trace is the one when inner plate detached as in right inset. Right inset also shows flat aluminium plate forming slit at centre, also the polygonal chain (green) depicting plane-wave path of WG mode

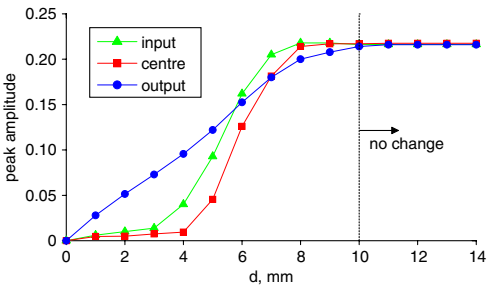

Fig. 6 *Peak positive amplitude of propagated signal as a function of slit opening d, formed at input, centre, and output of curved plate (no change in signal after 10 mm)*

Following an established theoretical analysis, we calculated the frequency-dependent propagation velocities and the spatial field profiles

(shown in Fig. 7) for the three lowest-order TE-type WG modes. We can relate the mode profiles to the intuitive bouncing-plane-wave picture depicted in the right inset of Fig. 5 using the (green) polygonal chain. For a given WG mode, as the frequency increases, energy is concentrated closer to the plate surface, consistent with a decreasing incidence angle for the plane wave, and therefore, a decreasing velocity. The frequency dependence of the velocity is quite gradual, and results in negligible dispersion, as observed in the undistorted pulse in Fig. 5. Further experimental and theoretical results indicate that for the cylindrical plate of radius 8 cm, the total propagation loss, combining both the ohmic loss and the diffraction loss, can be as low as 2.6 dB/m in the THz range [17].

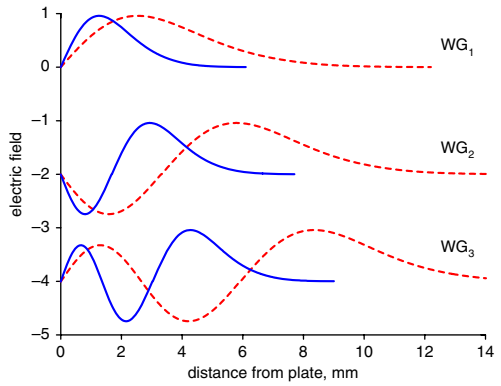

Fig. 7 *Spatial electric field profiles of three lowest-order TE-type WG modes at 0.1 THz (dashed curves) and 0.3 THz (solid curves) based on theory (profiles vertically offset for clarity)*

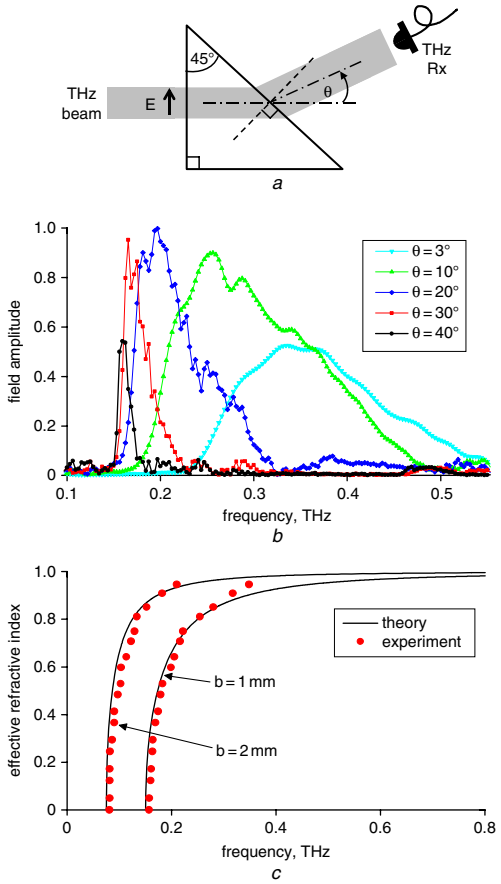

Fig. 8 *Schematic of PPWG prism; amplitude spectra; effective refractive index*

a Schematic of PPWG prism
b Amplitude spectra corresponding to THz signals detected at various Rx (angular) positions
c Comparison of experimental and theoretical effective refractive index

Artificial dielectrics: As already mentioned, the undesirable dispersive effect has discouraged the use of the TE_1 mode for THz pulse propagation in the past. However, we demonstrate that this dispersive effect can in fact be gainfully exploited to convert a PPWG structure into a 2D artificial dielectric medium with unique properties.

Using the well-known expression for the frequency-dependent phase velocity of the TE_1 mode, we can derive an effective refractive index as

$$n = \sqrt{1 - \left(\frac{f_c}{f}\right)^2} \tag{1}$$

This implies that n is close to unity at high frequencies, and reaches zero as the frequency decreases to the cutoff-frequency f_c. Therefore, a wave propagating in the TE_1 mode inside the PPWG experiences an effective medium with $0 \leq n < 1$ [18].

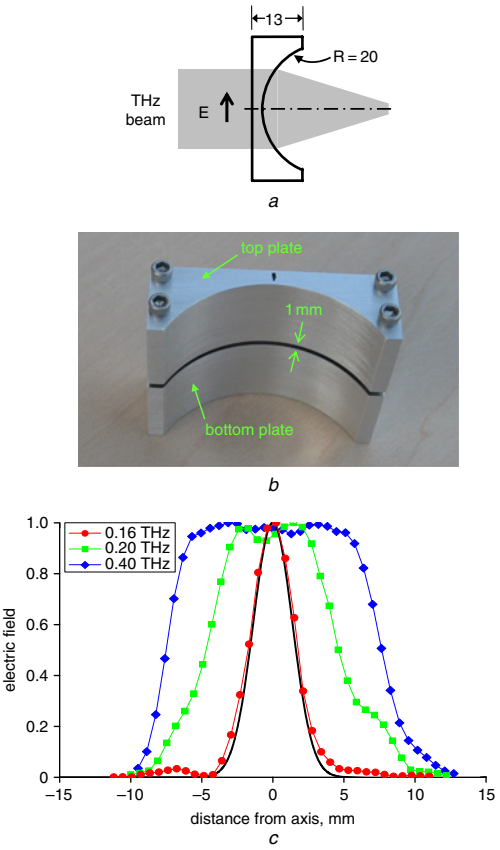

Fig. 9 *Schematic of PPWG-lens; photograph of fabricated device; derived experimental electric field profiles*

a Schematic of PPWG-lens (dimensions in mm)
b Photograph of fabricated device indicating 1 mm gap between two plates
c Derived experimental electric field profiles for frequencies of 0.16, 0.20, 0.40 THz at transverse plane 35 mm from front face
Solid black curve is theoretical Gaussian profile for 0.16 THz

To confirm this frequency-dependent behaviour of n, we used a 45° PPWG-prism as shown in Fig. 8*a*. A THz beam was coupled in at normal incidence, propagating via the TE_1 mode inside the prism. This beam encountered the exit face at an oblique angle of 45° and experienced a sudden change in index. In keeping with Snell's law, since the beam travels from a low-index ($n < 1$) medium to a high-index free-space ($n = 1$), the beam should bend towards the normal to the exit face. To test this experimentally, we detected the output signal by positioning the receiver along an arc, equidistant from the axial exit point. The amplitude spectra corresponding to the signals detected at various angular positions (θ) are shown in Fig. 8*b*, for a PPWG-prism with $b = 1$ mm. This shows a dramatic down-shifting of the spectrum towards low frequencies as θ increases from 0°, reaching frequencies near f_c at 45°. This behaviour is consistent with the aforementioned frequency dependence of n. The experimental behaviour is plotted in Fig. 8*c* by the dots, in comparison to the theoretical curve derived using (1), and shows very good agreement, confirming the artificial-dielectric concept. The dual-plate nature of the PPWG limits this medium to 2D. To extend this into the third dimension, we can use a stacked set of thin parallel metal plates. However, true 3D behaviour

is not possible since there cannot be any propagation normal to the plates.

Using this artificial-dielectric concept, we have fabricated a convergent PPWG-lens (see Figs. 9*a* and *b*). Since the medium has an index less than unity, to achieve a positive lensing effect, one needs to use a concave geometry, rather than the usual convex geometry employed with conventional dielectrics. Therefore, the lens was designed with a plano-concave geometry, and fabricated using two polished aluminium plates with $b = 1$ mm.

As the THz beam propagates through the lens, it undergoes focusing only along the direction parallel to the (inside) plate surfaces, while the output beam diffracts in the perpendicular direction. Since different frequencies experience different refractive indices, the focal-length is frequency dependent, and can be shown to vary from about 35 mm at 0.16 THz (near cutoff) to about 200 mm at 0.4 THz, as calculated from Gaussian-beam analysis. We mapped the transverse profiles of the output beam by scanning a 1 mm slit aperture, positioned 35 mm away from the front face. These results are shown in Fig. 9*c* for the frequencies of 0.16, 0.20, and 0.40 THz. The theoretical Gaussian profile at 0.16 THz is also shown for comparison, and shows excellent agreement. At 0.16 THz, the 20 mm ($1/e$ full-width) input beam size is focused to approximately 4 mm, and demonstrates the strong focusing power of this PPWG-lens.

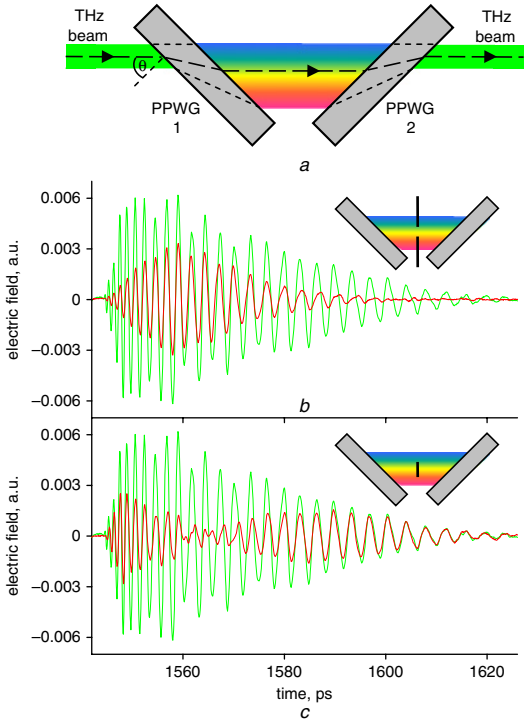

Fig. 10 *Device geometry showing two complementary PPWGs; typical time-domain output signal and reference in bandpass configuration, and in band-stop configuration*

a Device geometry showing two complementary PPWGs
Spatial frequency spread schematically indicated by 'rainbow' colours, where high-frequency components are towards blue side, while low-frequency components are red bottom side
b Typical time-domain output signal (red) and reference (green) in *band-pass* configuration, where metallic slit positioned between PPWGs as shown in inset
c Typical time-domain output signal (red) and reference (green) in *band-stop (or notch)* configuration, where metallic strip positioned between PPWGs as shown in inset

Universal THz filter: We can also exploit the unique dispersive behaviour characteristic of the artificial-dielectric concept to create a versatile spectral filter for broadband THz pulses [19]. The device geometry consists of two complementary PPWGs as shown in Fig. 10*a*. The input THz beam is incident on $PPWG_1$ at an oblique angle, and excites the TE_1 mode. Because different frequencies experience different refractive indices inside the waveguide, Snell's law dictates that the direction of propagation inside the waveguide is frequency dependent. Since the index decreases monotonically from unity to zero as the frequency decreases, the beam exiting $PPWG_1$ is spatially chirped. The high-frequency components lie closer to the input optic-axis and the low-frequency components are displaced from the optic-axis. The spatially spread beam is then coupled into an identical $PPWG_2$ that is in a complementary geometry. This reverses the chirp and combines the different frequency components back into a single output beam. By blocking portions of the spatially chirped beam between the two PPWGs, we can carry out various spectral filtering functions, effectively realising a 'universal' filter.

We demonstrate a *bandpass* and a *band-stop* filter by positioning a metallic *slit* and a metallic *strip*, respectively, between the two waveguides, as shown in the insets of Figs. 10*b* and *c*. In both Figures, the red trace shows the time-domain THz output signal, while the green trace shows the unblocked reference signal. In Fig. 10*b*, we see a progressive decrease in amplitude going towards the leading (high-frequency) and trailing (low-frequency) ends of the signal from the centre (mid-band), indicating a clear bandpass behaviour. In contrast, in Fig. 10*c*, there is a progressive decrease in amplitude going towards the centre from the leading and trailing ends, indicating a clear band-stop behaviour. We can also easily demonstrate lowpass and highpass behaviour, simply by blocking either the high-frequency or the low-frequency end, and even tune the respective cutoff frequencies by moving the (metallic) beam block. This spectral filter is reminiscent of the four-prism sequence commonly used in femtosecond pulse optics, and opens the possibility of numerous similar applications for THz pulses such as dispersion control or pulse shaping.

Conclusion: We have presented a review of our recent work utilising the TE_1 mode of the PPWG, which adds a whole new dimension to the multifaceted THz applications made possible by the PPWG. We anticipate that TE_1-mode parallel-plate wave guiding will play an important role in numerous future implementations of THz technologies.

21 September 2010
doi: 10.1049/el.2010.3318

R. Mendis and D.M. Mittleman (*Department of Electrical and Computer Engineering, Rice University, Houston, TX 77005, USA*)

References

1 Mendis, R., and Grischkowsky, D.: 'Undistorted guided-wave propagation of subpicosecond terahertz pulses', *Opt. Lett.*, 2001, **26**, pp. 846–848
2 Mendis, R., and Grischkowsky, D.: 'THz interconnect with low loss and low group velocity dispersion', *IEEE Microw. Wirel. Compon. Lett.*, 2001, **11**, pp. 444–446
3 Cao, H., Linke, R.A., and Nahata, A.: 'Broadband generation of terahertz radiation in a waveguide', *Opt. Lett.*, 2004, **29**, pp. 1751–1753
4 Coleman, S., and Grischkowsky, D.: 'Parallel plate THz transmitter', *Appl. Phys. Lett.*, 2004, **84**, pp. 654–656
5 Mendis, R.: 'Guided-wave THz time-domain spectroscopy of highly doped silicon using parallel-plate waveguides', *Electron. Lett.*, 2006, **42**, pp. 19–21
6 Melinger, J.S., Laman, N., Harsha, S.S., and Grischkowsky, D.: 'Line narrowing of terahertz vibrational modes for organic thin polycrystalline films within a parallel-plate waveguide', *Appl. Phys. Lett.*, 2006, **89**, p. 252220
7 Melinger, J.S., Harsha, S.S., Laman, N., and Grischkowsky, D.: 'Guided-wave terahertz spectroscopy of molecular solids', *J. Opt. Soc. Am. B*, 2009, **26**, pp. A79–A89
8 Zhang, J., and Grischkowsky, D.: 'Waveguide THz time-domain spectroscopy of nm water layers', *Opt. Lett.*, 2004, **19**, pp. 1617–1619
9 Nagel, M., Forst, M., and Kurz, H.: 'THz biosensing devices: fundamentals and technology', *J. Phys., Condons. Matter*, 2006, **18**, S601–S618
10 Awad, M.M., and Cheville, R.A.: 'Transmission terahertz waveguide-based imaging below the diffraction limit', *Appl. Phys. Lett.*, 2005, **86**, p. 221107
11 Musheinesh, M.A., Divin, C.J., Fessler, J.A., and Norris, T.B.: 'Time-reversal and model-based imaging in a THz waveguide', *Opt. Express*, 2009, **17**, pp. 13663–13670
12 Cooke, D.G., and Jepsen, P.U.: 'Optical modulation of terahertz pulses in a parallel plate waveguide', *Opt. Express*, 2008, **16**, pp. 15123–15129
13 Zhan, H., Mendis, R., and Mittleman, D.M.: 'Superfocusing terahertz waves below $\lambda/250$ using plasmonic parallel-plate waveguides', *Opt. Express*, 2010, **18**, pp. 9643–9650
14 Mendis, R., and Mittleman, D.M.: 'Comparison of the lowest-order transverse-electric (TE_1) and transverse-magnetic (TEM) modes of the parallel-plate waveguide for terahertz pulse applications', *Opt. Express*, 2009, **17**, pp. 14839–14850

15 Mendis, R., and Mittleman, D.M.: 'An investigation of the lowest-order transverse-electric (TE_1) mode of the parallel-plate waveguide for THz pulse propagation', *J. Opt. Soc. Am. B*, 2009, **26**, pp. A6–A13
16 Mendis, R., Astley, V., Liu, J., and Mittleman, D.M.: 'Terahertz microfluidic sensor based on a parallel-plate waveguide resonant cavity', *Appl. Phys. Lett.*, 2009, **95**, p. 171113
17 Mendis, R., and Mittleman, D.M.: 'Whispering-gallery-mode terahertz pulse propagation on a curved metallic plate', *Appl. Phys. Lett.*, 2010, **97**, p. 031106
18 Mendis, R., and Mittleman, D.M.: 'A 2-D artificial dielectric with $0 < n < 1$ for the terahertz region', *IEEE Trans. Microw. Theory Tech.*, 2010, **58**, pp. 1993–1998
19 Mendis, R., Nag, A., Chen, F., and Mittleman, D.M.: 'A tunable universal THz filter using artificial dielectrics based on parallel-plate waveguides', *Appl. Phys. Lett.*, 2010, accepted for publication
20 Laib, J.P., and Mittleman, D.M.: 'Temperature-dependent terahertz spectroscopy of liquid *n*-alkanes', *J. Infrared Millim. THz Waves*, 2010, **31**, p. 1015